Evaluating seasonal hydrological extremes in mesoscale (pre-)Alpine basins at coarse 0.5° and fine hyperresolution

Joost Buitink[1], Remko Uijlenhoet[1], and Adriaan J. Teuling[1]

[1]Hydrology and Quantitative Water Management Group, Wageningen University, Wageningen, The Netherlands

Correspondence: Joost Buitink (joost.buitink@wur.nl)

Abstract. In this study, we investigate the effect of model resolution on the simulated hydrological response in five mesoscale basins in the Swiss Alps using the distributed hydrological model Spatial Processes in Hydrology (SPHY). Model simulations are performed at resolutions matching regional scale (500×500 m, also matching "hyperresolution") and global scale modeling (40×40 km, matching a 0.5×0.5° pixel). The simulated response is investigated for four seasonal extremes, selected based on

5 temperature and precipitation anomalies. Results from the high resolution model show that the intra-basin response covers a large range of anomalies, often with contrasting anomaly signs. The intra-basin response was grouped by land cover, where different dominant runoff generating processes are driving the differences between these groups. The low resolution model failed to capture the diverse and contrasting response from the high resolution model, since both the complex topography and land cover classes were not properly represented. We show that the hydrological response simulated with a high resolution

10 model can be a lot more extreme than a low resolution model might indicate, which has important implications for global assessments carried out at their typical 0.5×0.5° resolution.

1 Introduction

In current distributed hydrological modeling, we identify two main different modeling approaches. On one hand studies are performed at global scale, and on the other hand studies are performed at regional or basin scales. The modeling approach

15 generally affects the choice of spatial resolution. Most global studies are ran at rather coarse spatial resolutions (often at 0.5×0.5°) to investigate trends in the terrestrial water cycle as result of recent and projected changes in climate conditions (e.g. Luterbacher et al., 2004; Sánchez et al., 2004; Barnett et al., 2005; Beniston et al., 2007; Sheffield and Wood, 2008; Adam et al., 2009; Sheffield et al., 2012; Van Huijgevoort et al., 2014; Jacob et al., 2014). These studies often rely on standardized values such as the Standardized Precipitation Index (SPI) in order to quantify differences between different climatic regions

20 across the globe. Although recent global hydrological models are slowly shifting from relatively coarse resolutions to very fine resolution (hyperresolution, ~1×1 km), this is not yet the state of the art (Wood et al., 2011; Bierkens, 2015; Bierkens et al., 2015). It is known that global simulations at high resolution improve predictions at small local scales (Bierkens et al., 2015). However, these global studies are limited by a lack of input data at hyperresolution or a lack of computational power (Beven and Cloke, 2012; Beven et al., 2015; Melsen et al., 2016b). As a result, most of the global studies are still performed at a

25 relatively coarse resolution. Even when global modeling at hyperresolution becomes state of the art, question remains how we

should deal with simulations at these fine spatial scales, since the models parameterizations are developed on a coarser scale (Clark et al., 2017; Peters-Lidard et al., 2017).

Another type of hydrological studies are those at basin or regional scales. These studies mostly use distributed hydrological models to simulate the hydrological response under climate change or climatic extremes (e.g. Middelkoop et al., 2001; Hurk-
5 mans et al., 2009; Driessen et al., 2010; Hurkmans et al., 2010; Wong et al., 2011; Immerzeel et al., 2012). Typical resolutions for these studies are similar to the previously mentioned hyperresolution or even finer. Since these studies have a narrower spatial focus than the global simulations, high resolution data is often easier accessible and the computational power is less of a limiting factor. Since differences are smaller within the region of interest, standardizing the results is often not required to have meaningful comparisons.

10 Both global and regional studies focus on reaching similar goals, yet with different methodologies. So far, no study has investigated how these two methodologies connect and how the modeling approach affects the results. The effect of model resolution on the simulated response has been investigated by numerous studies, either for regional climate models or for hydrological models (e.g. Haddeland et al., 2002; Leung and Qian, 2003; Carpenter and Georgakakos, 2006; Gao et al., 2006; Lucas-Picher et al., 2012; Pryor et al., 2012; Lobligeois et al., 2014; Kumar et al., 2016; Melsen et al., 2016a). However, no
15 study has investigated how anomalies in the simulated hydrological response depend on the modeling approach.

Since many hydrological processes are nonlinear or depend on thresholds, we expect that the modeling approach can greatly affect the model results. These nonlinearities and thresholds imply that a small change in input data or initial conditions can lead to relatively large changes in hydrological response. Scaling of these processes over heterogeneous catchments might therefore not be trivial when changing the spatial resolution. For example, Blöschl et al. (2013) investigated the 2013 flood of
20 the Danube river caused by extremely heavy precipitation. They found that the discharge peak could have been higher, since not all precipitation fell as rain. In parts of the catchment that were high enough for the temperature to stay below zero degrees Celsius, a fraction of precipitation fell as snow and did not directly contribute to the discharge. Teuling et al. (2013) showed that evaporation increased during droughts, based on data from several headwater catchments in Europe. This was explained by the lack of rainfall coinciding with reduced cloud cover and increasing net radiation, which out-weighted the effect of lower
25 soil moisture conditions. Jolly et al. (2005) studied how vegetation responded to the extreme summer of 2003 in the Swiss Alps. They found that vegetation response was not homogeneous, but showed different responses per elevation zone. Finally, catchments in the Swiss Alps are known to show complex behavior due to the non-trivial response of snow and glaciers to extreme events (Verbunt et al., 2003; Zappa and Kan, 2007; Van Tiel et al., 2018). These examples indicate the complexity of the hydrological response and the variability in time and space in these regions.

30 In this study, we aim to investigate how the simulated hydrological response depends on model resolution, by using two commonly used spatial resolutions. Model results at a typical resolution for regional scale models (~500×500 m, also matching "hyperresolution") are compared to model results at a typical resolution for global scale models (~40×40 km, matching a 0.5×0.5° pixel). We focus on the Swiss Alps, due to their large variation in land cover and elevation, and due to the vast knowledge of this region (e.g. Gurtz et al., 2003; Verbunt et al., 2003; Jolly et al., 2005; Schaefli et al., 2007; Zappa and Kan, 2007;
35 Bavay et al., 2013; Speich et al., 2015). We study the response of five basins to four seasons by simulating each basin with the

Hydrology and
Earth System
Sciences
Open Access
Discussions

Table 1. Statistics for each catchment (FOEN, 2016).

Main river basin	Reuss	Rhone	Inn	Emme	Thur
FOEN station ID	2056	2346	2403	2155	2181
Name outlet station	Seedorf	Brig	Cinuos-chel	Wiler	Halden
Outlet elevation [m a.s.l.]	438	667	1680	458	456
Surface area [km^2]	832	913	736	940	1085
Mean elevation [m a.s.l.]	2010	2370	2467	860	910
Glaciation [%]	9.5	24.2	8.5	0.0	0.01

Spatial Processes in Hydrology model (SPHY) at both resolutions. The four seasons were selected based on unusual precipitation and/or temperature values (hereafter referred to as "extreme seasons"). We hypothesize that the spatial resolution will play an important role in the simulated response, since many hydrological processes during extremes are inherently nonlinear combined with the fact that most of the variability occurs at scales smaller than the spatial resolution of global hydrological

5   models.

2   Methods, model and data

2.1   Basins

For this study, we selected five mesoscale basins in the Swiss Alps. Not only is the response of these basins relevant at regional scale, these basins also contribute considerable amounts to large rivers in Europe. For example, the discharge of the Rhine

10   consisted for almost 40% of melt water from the Swiss Alps during the warm and dry summer of 2003 (Wolf et al., 1999; Stahl et al., 2016). While not all basins are tributaries to the Rhine, they nonetheless provide important insight into our understanding of the behavior of mountainous catchments. The basins for our study were selected based on size (roughly corresponding to the 0.5°×0.5° pixel size), elevation range, land cover, human influence and data availability. Figure 1 shows the locations and digital elevation models of all catchments. Please note that not always the entire river basin is chosen; see Table 1 for the names,

15   station identifiers used by Swiss Federal Office of the Environment (FOEN) and other characteristics. Two basin categories can be distinguished: high-elevation catchments with glaciers (Reuss, Rhone and Inn) and lower-elevation catchments without glaciers (Emme and Thur). We will refer to those basin categories as Alpine and pre-Alpine, respectively.

2.2   Data

The model is forced with daily precipitation and temperature from MeteoSwiss (MeteoSwiss, 2013, 2016). All forcing data

20   is provided at a resolution of approximately 2×2 km Land cover data was obtained from WSL (2016) and grouped into four classes: forest, grass, glacier and other. The latter class combines all sparse vegetation types, bare soil and rocks. Discharge
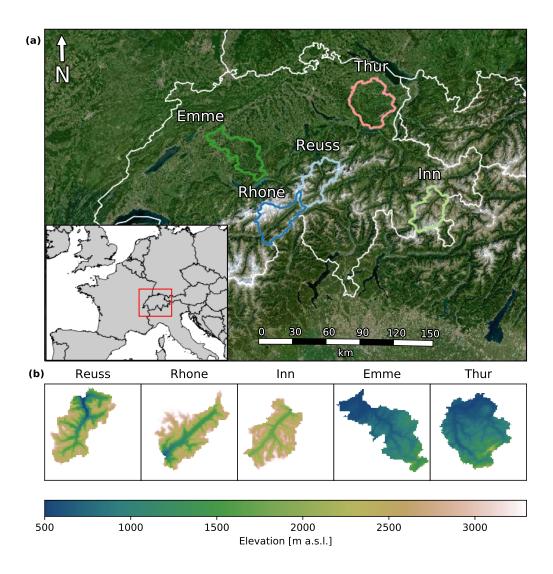
Figure 1. Overview of the location (a) and elevation (b) of the five basins used in this study. Names of the main river basin are plotted above the catchment border in (a). Each box in (b) corresponds to an area of ~40×40 km.

observations are obtained from FOEN (2016). Catchment elevation, delineation and stream network are derived from the digital elevation model of Jarvis et al. (2008).
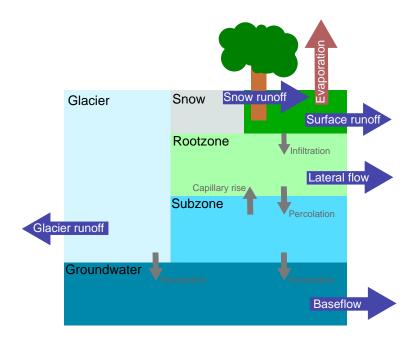
2.3 Hydrological model

The Spatial Processes in Hydrology model (SPHY) was used to simulate each basin at both resolutions. SPHY is a spatially
5 distributed conceptual hydrological model, including representations of rainfall-runoff, cryosphere, evapotranspiration and soil moisture processes, as well as their nonlinearities and thresholds (Lutz et al., 2013, 2014; Terink et al., 2015; Lutz et al.,
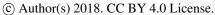
Figure 2. Schematic overview of the conceptualization in SPHY. Blue arrows represent fluxes contributing to total runoff generated in each model cell and small grey arrows represent fluxes between the different reservoirs. Overview is based on the more detailed concept by Terink et al. (2015).

2016; Hunink et al., 2017). The model runs on a daily time step and a user-defined spatial resolution. Sub-grid variability is taken into account via cell fractions, but only for snow and glacier fractions. A schematic overview of the model concept is presented in Fig. 2. Based on the daily average temperature, SPHY determines whether precipitation will fall as snow or rain. The liquid precipitation will fall on the land surface, where part of the water can be directed to the river as surface runoff,

5   depending on the volume of water already present in the rootzone. The remainder infiltrates into the rootzone, where it is subject to evapotranspiration based on the type of land cover. Water in the rootzone can either percolate to the subzone, or is transported to the river network as lateral flow. From the subzone, water can either move upward into the rootzone as result of capillary rise, or can percolate to the groundwater layer. Water in the groundwater layer will contribute to the river discharge as baseflow. Solid precipitation is added to the snow storage, where melting of snow is diverted to the stream network as snow

10   runoff. Finally, part of the grid cell can consist of glaciers. A fraction of the melted ice is added to the groundwater storage, and another fraction is transported to the river as glacier runoff. The glaciers in SPHY are fixed in space and time, so glaciers cannot extend and retreat. More information about the model structure and parameterizations are provided by Terink et al. (2015).

2.4 Model setup and calibration

SPHY was applied to each basin at two different resolutions: at ~500×500 m (corresponding to the regional scale resolution, and "hyperresolution"), and at ~40×40 km (corresponding to the global scale resolution of 0.5°×0.5°). This latter resolution implies that each basin was simulated as a single pixel. All input data were re-sampled to match the spatial resolution of the hydrological model. For the high resolution model we used bilinear interpolation to resample the forcing data for the high resolution model, and we averaged all cells within the 40×40 km pixel for the low resolution model. SPHY was calibrated individually for both resolutions and all basins using the L-BFGS-B algorithm (Zhu et al., 1997), by minimizing the sum of squares of the residuals between monthly simulated and observed discharge. SPHY was calibrated over a period of five years (1997-2001), where the preceding year was used as spin-up period. These years were chosen to include both a relatively wet year (1999) and two relatively dry years (1997 and 1998). Four parameters were selected for calibration, all of which were found to influence the monthly discharge: rootzone depth, degree-day factor for snow melt, a parameter determining the fraction of water that can refreeze in the snow pack, and the critical temperature describing the point where precipitation falls as snow. Since the L-BFGS-B algorithm is highly sensitive to the initial parameter guess, 10 different starting parameters sets were generated using Latin Hypercube Sampling to cover the parameter space (McKay et al., 1979). The calibration resulted in 10 new parameter sets per region and model type, and we selected the parameter set with the highest Kling-Gupta efficiency (Gupta et al., 2009). Using this parameter set, SPHY was ran from 1993 to 2014, where the first year was used as a spin-up period, resulting in 21 years of data used for analysis.

2.5 Anomalies and metrics

In this study, we only focus on the runoff and actual evaporation responses. We averaged all model output over three months, grouping the hydrological response per season: December, January and February for winter (DJF); March, April and May for spring (MAM); June, July and August for summer (JJA); September, October, November for autumn (SON). Standardized anomalies are used to quantify the magnitude of the deviation within each season, and are calculated for each individual model cell, using the following equation:

$$Z_{xi}^S = \frac{x_i^S - \mu_x^S}{\sigma_x^S}, \tag{1}$$

where μ_x^S is the mean of variable x in season S, x_i^S is the value of variable x for year i in season S, σ_x^S is the standard deviation of x based on the same period, and Z_{xi}^S is the dimensionless standardized anomaly of variable x for year i in season S. We note that most often climatologies are calculated based on time series of 30 years or more. We were not able to generate 30 years of data, because we only had sufficient data for the period 1993-2014. Since the focus of this paper is not on the absolute values, but on the patterns and relations, we do not expect different conclusions when longer time series would have been used.

Since the goal of this paper is to compare results from a high resolution model with results from a low resolution model, we require a suitable metric to quantitatively evaluate the difference between those results. Based on the previously discussed methodology, the high resolution model outputs a distribution of values, which needs to be evaluated against a single value

from the low resolution model. Ideally, the metric provides robust information regardless of the shape of the distribution of the results from the high resolution model. A common option would be to calculate the percentile score of the low resolution model result within the high resolution model results. However, the percentile score does not provide information about the size of the error between the high and low resolution models. Another option would be the root mean square error (RMSE).

5   The RMSE can be rewritten in terms of mean and variance, resulting in the following equation:

$$\text{RMSE} = \sqrt{\sigma^2 + (\mu - Z_{\text{low\_res}})^2}, \tag{2}$$

where σ^2 and μ are the variance and mean of the (normalized) high resolution model results and $Z_{\text{low\_res}}$ is the low resolution model result. However, when working with skewed or bimodal data (as visible in Fig. 9), the mean and variance are not sensible measures to describe the distribution of values.

10   Therefore we propose a new metric, which provides a measure of the distance between a single point and a distribution of values, regardless of the shape of the distribution, and that not only includes information on the difference in mean or median, but also on the width of the underlying distribution that the single value tries to represent. We call this new metric the Density Weighted Distance (DWD). DWD measures the distance between a single point and a range of values, weighted by the density of data that is present between the single point and the extent of the range of values. The extent is measured as the $5-95\%$

15   range to exclude the outliers, and the distances between the single point and the minimum and maximum extent are multiplied by the percentile of data within this distance. DWD is defined as follows:

$$\text{DWD} = (P_{\text{low\_res}} - 0.05) \cdot d_{\text{lower}} + (0.95 - P_{\text{low\_res}}) \cdot d_{\text{upper}}, \tag{3}$$

with d_{lower} and d_{upper} defined as

$$d_{\text{lower}} = Z_{\text{low\_res}} - Z_{\text{high\_res}}^{5\%}, \tag{4}$$

20    $$d_{\text{upper}} = Z_{\text{high\_res}}^{95\%} - Z_{\text{low\_res}}, \tag{5}$$

where d_{lower} and d_{upper} are the distances between the low resolution model result ($Z_{\text{low\_res}}$) and the 5% and 95% results from the high resolution model ($Z_{\text{high\_res}}^{5\%}$ and $Z_{\text{high\_res}}^{95\%}$, respectively). $P_{\text{low\_res}}$ is the percentile of $Z_{\text{low\_res}}$ within $Z_{\text{high\_res}}$. The DWD concept is visualized in Fig. 3a.

The DWD can be interpreted as the difference in terms of number of standardized anomalies. DWD is zero when the high

25   resolution data has zero variability, and when the difference with the low resolution model results is also zero. If the high resolution data has zero variability, but the result from the low resolution model is outside of this range, DWD will give the distance between the low and high resolution data, measured in number of standardized anomalies (see the "Flat" subplot in Fig. 3b.).

In order to illustrate the concept behind DWD and compare it to the previously mentioned metrics, Fig. 3b shows the different

30   metrics using four synthetic example. The example with the "Flat" distribution assumes no variability in the high resolution model results. As a consequence, the violin plot is a horizontal line. Since there is no variability in the high resolution model results, RMSE and DWD give the same values. The percentile value is equal to zero, since the low resolution model result is
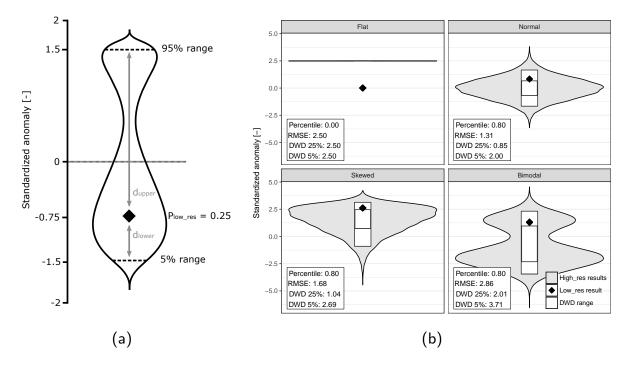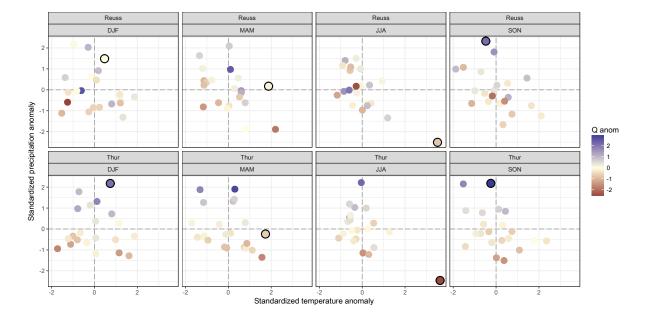
Figure 3. The concept behind Data Weighted Distance (a) and comparison between different metrics (b). Substituting the values from (a) into Eq. (3) gives the following result: $DWD = (0.25 - 0.05) \cdot 0.75 + (0.95 - 0.25) \cdot 2.25 = 1.725$. In (b), the violin plots represent the distribution of the high resolution model results and the diamond the single low resolution data point. The large box in (b) represents the $5 - 95\%$ data range, and the smallest box the $25 - 75\%$ data range.

outside of the high resolution model results. The three other examples in Fig. 3b illustrate that the percentile score does not give sufficient information to draw conclusions about the performance of the low resolution model, since they all received the same percentile score. The RMSE is able to catch the differences between the last two cases, but it does not accurately display the distance between the range of data from the high resolution model and the single point from the low resolution model.

5   Furthermore, when working with skewed or bimodel data, the mean and variance are not the best indicators for the distribution of values. In contrast, DWD combines the spread of the high resolution results with the density of data points, resulting in a more sensible measure when dealing with skewed or bimodal data. We also compared the effect of selecting a different data range: $25 - 75\%$ instead of $5 - 95\%$. We conclude that this mostly influences results in terms of absolute size, but does not alter the relative differences much. We expect that when using the $25 - 75\%$ range, low resolution model results will be more

10   often outside of this range than when using the $5 - 59\%$ range. Furthermore, we assume that all grid cells in the high resolution model are equally important and will therefore use the largest data range to calculate the DWD, only excluding the outer 10% to remove any undesired behavior resulting from outliers.

Hydrology and
Earth System
Sciences
Discussions

Figure 4. Relation between climate anomalies and observed and simulated anomalies in hydrological response. Each dot represents a single season and is colored with the standardized observed discharge anomaly. Dots with black outline represent the selected extreme seasons (winter of 1995, spring of 2007, summer of 2003 and autumn of 2002).

3 Results and discussion

3.1 High resolution simulations

The key focus of this work is the catchment response to extreme seasons. To identify those extreme seasons, standardized precipitation and temperature anomalies are calculated for each season and basin (see Fig. 4). Since patterns are similar across the two catchment types, results of only two basins are shown in this figure. It should be noted that due to averaging values over three months, it is very likely that extreme events with a shorter duration are averaged out in this three-monthly time step.

The highlighted dots in Fig. 4 show the extreme seasons selected for this study, for which the hydrological response is analyzed. The seasons were selected based on unusual precipitation and/or temperature values: winter of 1994/95, spring of 2007, summer of 2003, autumn of 2002. Brönnimann et al. (2007) and MeteoSwiss (2017) both mention the high temperature during the spring of 2007 in Switzerland. The extremely warm and dry summer of 2003 is known to be the most extreme summer in at least the last 500 years (Luterbacher et al., 2004; Zappa and Kan, 2007; Seneviratne et al., 2012). The extremely heavy precipitation during November 2002 caused mudflows in eastern Switzerland (Schmidli and Frei, 2005). No literature reference was found for the unusually wet winter of 1994/95.
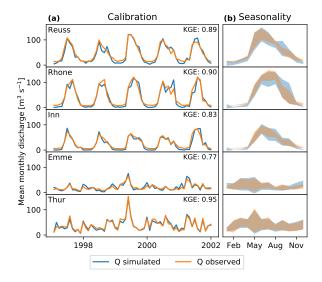
The colors of the circles indicate the discharge anomalies. Discharge anomalies in the pre-Alpine basin seem to follow a distinct pattern, where high precipitation values often coincide with high positive discharge anomalies, and vice versa. Tempe-

Figure 5. Discharge observations compared with discharge simulations for (a) the calibration period and (b) the monthly average discharge. In the top right corner of each subplot in (a), the Kling-Gupta efficiency (KGE) is presented. The range in (b) is plotted as the standard deviation around the mean monthly discharge.

rature also seems to influence discharge anomalies in the pre-Alpine basin, but this relation is less evident. The Alpine basin shows a much more random pattern, without any clear relation between temperature and/or precipitation. This indicates that the runoff generating processes are not consistently driven by either precipitation or temperature, but by a combination of both.

    The calibration results for each basin are presented in Fig. 5a. This figure shows high Kling-Gupta efficiencies for all basins,

5 indicating good model performance. Overall, the peaks are simulated at the correct time and magnitude. Only the winter discharge in the Alpine basins is underestimated by the model. Discharge observations show an almost constant outflow during winter, which is most likely the result of human interference (reservoirs). SPHY is not able to simulate this constant outflow and simulates discharge values close to zero. As a means of validating the model, we presented the seasonality of each basin in Fig. 5b. In each basin, the seasonality is very well captured by the model, ensuring the (seasonal) patterns are well captured

10 by the model.

    Hydrological response maps for the two main hydrological fluxes (actual evapotranspiration (ET) and generated runoff) during each extreme season are presented in Fig. 6. Grid cells are colored by their cell-specific standardized anomalies. ET anomaly maps are only shown for spring and summer periods, when this flux is most important. During the two other seasons, large parts of the basins are covered with snow, where the model assumes no ET to occur. The same maps on a monthly time

15 step are presented in Appendix A. All basins show roughly the same ET response to the warm spring conditions in 2007. In the areas with a standardized anomaly of exactly zero, no evapotranspiration was simulated since the cells were covered with snow. Cells close to this region show a particularly high standardized anomaly. These cells are free of snow only for a limited time during spring, distorting the mean and standard deviation used to calculate the standardized anomaly.
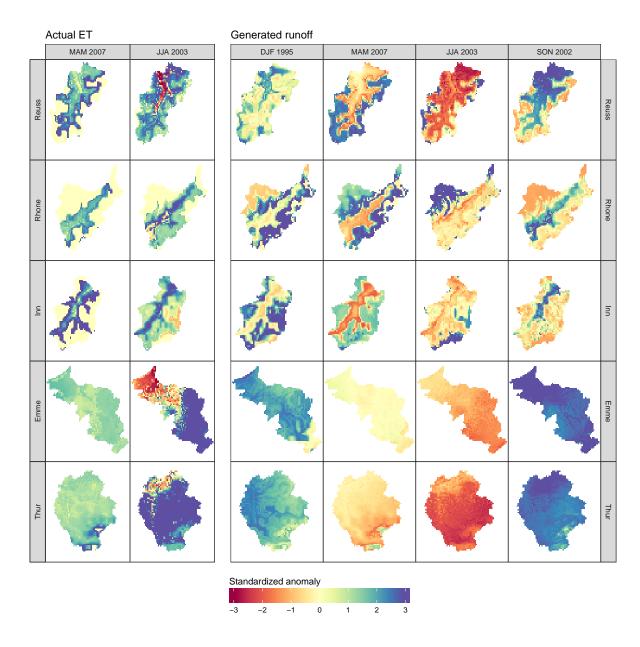
Figure 6. Spatial distribution of anomalies of actual evapotranspiration (a) and generated runoff (b) during the four extreme seasons, for all basins. The location of each catchment can be found in Fig. 1. Each box represents a size of ~40×40 km.

A more complex response is visible during the extremely warm and dry summer of 2003. In three basins, cells at low elevations show a different anomaly sign than the cells at mid/high elevations. In the entire region, higher temperatures increased the potential evapotranspiration, yet cells with a negative anomaly evaporated less water than normal. This indicates that those cells became water-limited during the course of the summer, and could no longer meet the potential ET. Cells at high elevations

were able to meet the increased potential ET, and evaporated a lot more water than normal. This lead to a situation in which both negative and positive anomalies are present within the same basin, even at seasonal timescale and in response to a rather homogeneous distribution of temperature anomalies. Only the Rhone and Inn basins did not show this behavior, indicating that the low elevation cells did not become water-limited over the course of this summer.

5   Anomalies in the generated runoff also show a contrasting within-basin response, in particular in the Alpine basins. Here, cells with low elevations show a different anomaly than the cells at high elevations. This dependency between anomaly and elevation is not visible in the pre-Alpine basins, where all model cells show roughly the same response. The cause of this difference between the two basin types will be further investigated below in Fig. 8. Previously, we mentioned that the unusually wet autumn of 2002 was mainly due to a period with unusually high precipitation in November. The anomalies of the other

10   seasons were mainly cause by a succession of multiple months with unusual temperature and/or precipitation values, so we chose to use a consistent time scale of three months throughout the paper. We also analyzed the hydrological response on a monthly timescale, but concluded that the response maps for November 2002 were not too different from the response maps for the autumn of 2002 (see Appendix A).

The spatial variability (as expressed by the standard deviation, σ) of both fluxes is plotted against the average forcing for

15   all seasons in Fig. 7. Here the standard deviation is used as a measure of complexity, with large σ values indicating a highly spatially variable and thus complex hydrological response. This figure gives insight into how the response complexity varies with basin average forcing. The precipitation - evapotranspiration plot was excluded since the graph consisted of random scatter, without a clear relation.

Spread in the actual evapotranspiration response seems related to temperature (Fig. 7a), where higher temperatures result in

20   larger ET standard deviations. As mentioned earlier, potential evapotranspiration will increase with higher temperatures, but so does the number of water stressed cells. This combination increases the spatial σ for evapotranspiration, and is visible in almost all basins and seasons.
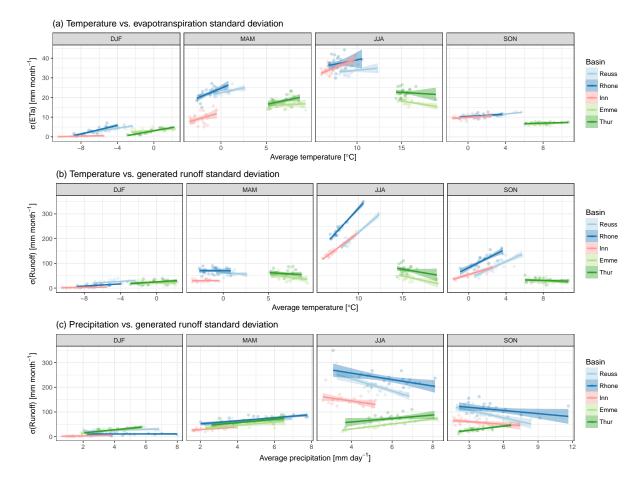
Standard deviation of generated runoff seems most sensitive to temperature during summer and autumn, see Fig. 7b. The two catchment types show a different response: the runoff σ increases with temperature in the Alpine basins, while runoff σ

25   decreases with temperature in the pre-Alpine basins. The cause for this difference is the presence of glaciers: glacier melt will increase with higher temperatures, while regions without glaciers will evaporate more. This contrast results in an increasing σ with temperature in the Alpine basins, and in a decreasing σ with temperature in the pre-Alpine basins. Please note that the average temperatures in both catchment types show hardly any overlap, making it difficult to identify how the basins would respond to the same temperature values.

30   Influence of average precipitation on the runoff σ seems smaller (Fig. 7c). However, in the simulation period we selected, there is a correlation between temperature and precipitation. During winter, only the pre-Alpine basins show a response in runoff σ to precipitation. The lack of response in the Alpine basins is related to temperature: the average winter temperatures in these basins hardly reaches values above 0°C, where precipitation will fall as snow and does not directly contribute to runoff. A more pronounced relation between precipitation and runoff σ is visible in summer and autumn, where σ in the Alpine

35   basins decreases with increasing precipitation and vice versa in the pre-Alpine basins. However, the Alpine regression lines

Hydrology and
Earth System
Sciences
Discussions

Figure 7. Relation between standard deviation (σ) of simulated hydrological response and basin-averaged weather conditions: temperature versus evapotranspiration σ (a), temperature versus runoff σ (b), precipitation versus runoff σ (c). Each point represents a single season in the 1994-2014 period. A linear regression through these points is represented as a solid line, with the shaded area indicating the 95% uncertainty range.
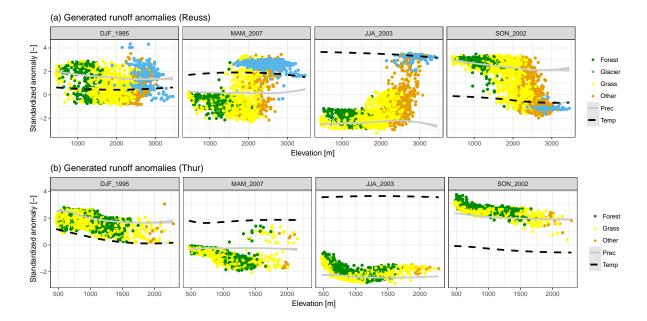
are strongly influenced by the extremely warm and dry summer of 2003: without this season, the regression lines would have been much more horizontal. Since there is only one season this extreme in the 21 years of simulations, it remains difficult to separate the effects induced by temperature or by precipitation. The autumn period shows a similar response as the summer months, but the relation with temperature needs to be taken into account again. As visible in Fig. 4, seasons with unusually high precipitation are often related to lower temperatures, while seasons with less precipitation are often paired with higher temperatures; independent of the basin. This could indicate that the relation between precipitation and runoff σ might be the inverse of the temperature - runoff σ relation.

To gain a better understanding about the hydrological behavior within each basin, the standardized anomalies of each individual grid cell are plotted against elevation in Fig. 8. We again only show results for one basin of each catchment type, since the

Figure 8. Relation between elevation and hydrological response colored by land cover type, presented for the Reuss (a) and Thur (b) basins. Each point represents the standardized anomaly for a single model cell, based on the data in Fig. 6. The solid and dotted lines show the smoothed precipitation and temperature anomalies, with the shaded area showing the 5−95% data range. Land cover type "other" represents all sparse and bare vegetation types.

response patterns were similar across the different basins. The forcing anomalies show very little spread: the 95% confidence interval is almost always thinner than the plotted line, making it barely visible. Spread in runoff anomalies is bigger than the spread in forcing anomalies in both catchment types, making it impossible to explain the hydrological response solely by the forcing anomalies. Each dot in Fig. 8 is colored by land cover. Land cover shows a clear correlation with elevation, best visible in the Alpine basin. The pre-Alpine basins did not contain any glacier cells and only a limited number of sparse/bare cells. This is explained by their more limited elevation range compared to the Alpine basins (see Fig. 1b).

The hydrological response can be grouped per land cover class: "forest" and "glaciers" show nearly always a different response within the same basin and season, where "grass" and "other" are covering a gradual transition between the two groups. This grouping can be explained by the runoff generating processes. Areas at high elevation generate runoff by melting ice and snow (if present), while areas at low altitudes rely on rootzone and/or groundwater processes. The latter are mostly driven by the amount of available water (water limited), while runoff from ice and snow is mostly dependent on the incoming energy (energy limited). This dependency is best visible in Fig. 8a, where the hydrological anomalies at lower elevations coincide with the sign and size of the precipitation anomaly, while hydrological response shifts towards the temperature anomaly at higher elevations. Due to the insufficient "other" and "glacier" cells in the pre-Alpine basin, this relation is not as evident as in the Alpine basin. In the pre-Alpine basin, runoff anomalies seem to follow precipitation anomalies, indicating that the runoff generating processes are mostly driven by available water (Fig. 8b). This grouping of different responses matches with

different zones defined by Theurillat and Guisan (2001): colline, < 700 m; montane, $700 - 1400$ m; subalpine, $1400 - 2100$ m; alpine, $2100 - 2800$ m; nival, > 2800 m. These zones match with the different land cover classes defined in our study: the first class is not represented in basin Reuss, montane corresponds to the "forest" group, subalpine to the "grass" group, alpine and nival to the "other" and "glacier" groups. A study by Jolly et al. (2005) described that these zones could also be used to group

5   vegetation responses to the extreme summer of 2003. This indicates that elevation and thus vegetation cover are controlling the hydrological response to extreme seasons.

     Our results may be influenced by parameterizations defined within the model. For example, the limited evapotranspiration of snow-covered cells is a choice made by the developer of SPHY. One could argue whether this is realistic. Furthermore, the glaciers in SPHY are fixed in location and extent. The importance of dynamical glaciers is investigated by Van Tiel et al.

10   (2018), and they conclude that using a dynamical glacier module is most important for long term studies. The simulation period of our study was rather short, and we therefore expect only minor differences in the location and extent of the glaciers over our time period. We do not expect any major different results and conclusions as result of those parameterizations within SPHY.

3.2   Impact of model resolution

With improved understanding of the hydrological response to extreme seasons when simulated at high resolution (matching the

15   regional scale studies), we can now compare those results to the model output when the basins are simulated on a $0.5° \times 0.5°$ resolution (matching the global scale studies). The different responses are presented in Fig. 9. In this figure, output from only two basins is shown since results were similar across basins of the same catchment type. High resolution model responses are clearly not normally distributed, but have a bimodal or skewed distributions. Response of the pre-Alpine basin shows less variation than the Alpine basin, which was also visible in Fig. 8. In all cases, the low resolution model anomaly is within the

20   high resolution model anomaly range, but does not show a consistent position within this range. This figure makes it difficult to quantify the differences between the low and high resolution models.
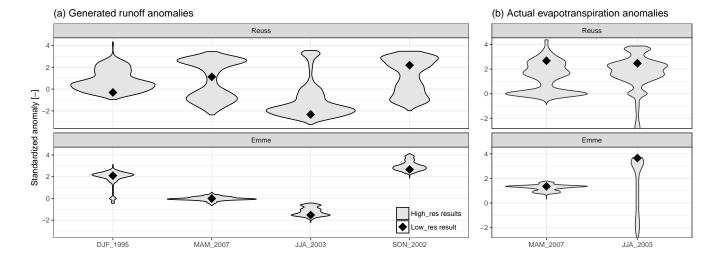
     For each hydrological flux, basin and extreme season, the Density Weighted Distance (DWD) is calculated and presented in Table 2. This table shows that the runoff DWD in the Alpine basins is generally higher than the DWD in the pre-Alpine basins (average Alpine $\mathrm{DWD} = 2.61$ and average pre-Alpine $\mathrm{DWD} = 0.81$). This is also visible in Fig. 9, where the pre-Alpine runoff

25   violin plots cover a smaller anomaly range than the Alpine violin plots. These averages indicate that the high resolution model anomalies can deviate with 2.61 and 0.81 standardized anomalies from the low resolution model anomaly in the Alpine and pre-Alpine basins, respectively. This illustrates that in these areas, the local hydrological response can be a lot more extreme than the low resolution model might indicate. This effect is largest in the Alpine basins, which can be explained by the wider range in elevation and land cover types.

30   The summer of 2003 in the Rhone basins shows a very high DWD value for the generated runoff ($\mathrm{DWD} = 4.32$). This is due to a combination of a relatively low percentile score ($\mathrm{P} = 0.18$) and a large distance to the upper 95% anomaly ($d_{\mathrm{upper}} = 5.57$). A very large portion of the high resolution model values is close to the low resolution model anomaly, implying that a small increase in low resolution model anomaly would significantly increase the $P_{\mathrm{low\_res}}$ values, which would have reduced the emphasis on d_{upper}, decreasing the DWD value, see Fig 9b.

Figure 9. Model response to extreme seasons for both generated runoff (a) and actual evapotranspiration (b), where violin plots represent the high resolution model response and the diamond the low resolution model response.

Table 2. Density Weighted Distance for both hydrological fluxes during the four extreme seasons, for all basins.

Basin	Total generated runoff				Actual ET	
	DJF 1995	MAM 2007	JJA 2003	SON 2002	MAM 2007	JJA 2003
Reuss	2.37	2.08	4.32	2.32	2.20	3.33
Rhone	2.58	2.54	3.86	1.69	0.76	1.37
Inn	2.16	1.64	4.11	1.66	3.94	1.97
Emme	1.12	0.30	0.71	0.91	0.41	5.66
Thur	0.87	0.66	1.33	0.60	0.56	4.12

Another high DWD value is found for actual evapotranspiration during the summer of 2003 in the Emme basin (see Fig. 9b). The high resolution model results show a long tail towards negative anomalies, caused by model cells which are water-limited during this season. The low resolution model is not able to replicate the response, since the model consisted of only a single grid cell. This cell was not water-limited during this season, since higher than average ET was simulated. As a result, the low

5 resolution model is not able to mimic basin responses which are as far as 5.66 standardized anomalies away from the low resolution model.

Actual evapotranspiration is not only dependent on the amount of available water, but snow cover is also an important factor. For example. the high DWD value for evaporation in the Inn basin during the spring of 2007 can be attributed to this response. In the low resolution model, the cell was free of snow, allowing the model to evaporate, while in the high resolution model only

10 half the cells were free of snow. The cells covered with snow were not able to evaporate water, resulting in a large variation in anomalies and thus a large $5 - 95\%$ range.

The results may be influenced by the fact that the model did not allow for sub-grid variability in land use or soil types, something other models might have included. When sub-grid variability is taken into account, we expect the low resolution model results to become less extreme. However, the low resolution model will not be able to capture the full dynamics simulated with the high resolution model, since landscape characteristics still need to be aggregated to a coarser resolution.

4   Summary and conclusions

In this study, we investigated the hydrological response anomalies in five catchments in the Swiss Alps at two different spatial resolutions. The catchments were selected based on topography and land cover. Three out of five catchments are situated at high elevations and contain glaciers (referred to as Alpine catchments), and the two other catchments are situated at lower elevations and do not contain glaciers (referred to as pre-Alpine basins). We ran the distributed hydrological model Spatial Processes in Hydrology (SPHY) at two different spatial resolutions to match two common hydrological modeling approaches: at a high resolution of ~500×500 m to match regional scale studies (and matching "hyperresolution"), and at a lower resolution of ~40×40 km to match global scale studies performed at 0.5×0.5° resolution. Model results were aggregated per season, and were analyzed based on standardized anomalies. For each season, we selected one season with unusual precipitation and/or temperature values within the simulation period of 1993-2014: winter of 1995, spring of 2007, summer of 2003 and autumn of 2002.

Results from the high resolution model show that the intra-basin response covers a large range of anomalies during the selected seasons, where contrasting anomaly signs within a single catchment are often occurring. Within-basin complexity of hydrological response was found to generally increase with the magnitude of the forcing anomaly. The low resolution model failed to capture this diverse and contrasting response, since the entire region was covered by a single grid cell. The newly introduced Density Weighted Distance (DWD) was used to quantify the difference between the high and low resolution models, and indicated that the low resolution model misses on average more than 2 standardized anomalies compared to the high resolution model. Our results show that results generated with a high resolution model are not only more variable, but anomalies can locally be much more extreme or even of the opposite sign than a low resolution model might indicate. This conclusion confirms previous results by Melsen et al. (2016a), who found that results of large-domain models should be interpreted with care because of a lack of spatial variability in these models. Since our low resolution model did not represented sufficient spatial variability, this led to a large discrepancy between the high and low resolution model results.
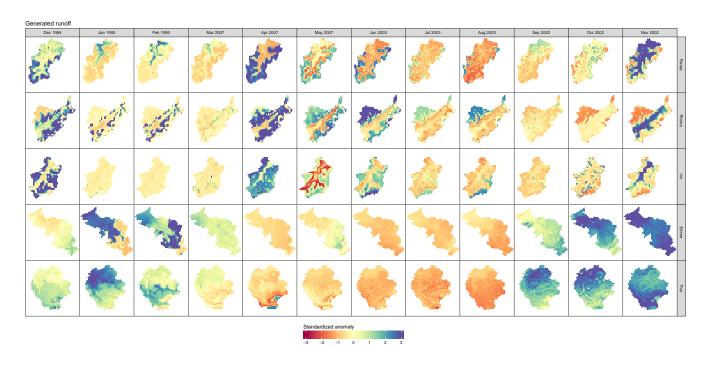
The variability in simulated response was associated with the different land cover classes. We found that runoff anomalies were matching the temperature anomalies when the dominant runoff generating processes are energy-limited (snow/glaciers), and runoff anomalies were matching precipitation anomalies when the dominant runoff generating processes are water-limited (grass/forest). The two pre-Alpine basins generally showed a different response than the Alpine basins, which can be attributed to the smaller variation in elevation and land cover in these basins. The grouping of responses in our study matches the elevation classes as defined by Theurillat and Guisan (2001).

Hydrology and
Earth System
Sciences

Open Access

EGU

Discussions

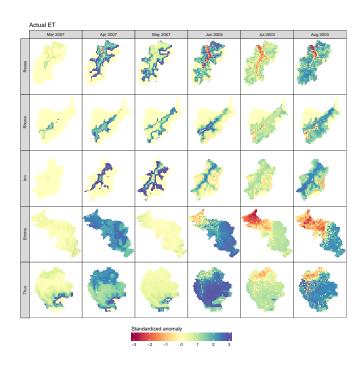# Appendix A: Monthly anomaly maps

Figure A1. Spatial distribution of monthly anomalies of generated runoff, during the months of the selected season. Each box represents an area of ~40×40 km.

Competing interests. The authors declare that they have no conflict of interest.

Figure A2. Spatial distribution of monthly anomalies of actual evapotranspiration, during the months of the selected season. Each box represents an area of ~40×40 km.

References

Adam, J. C., Hamlet, A. F., and Lettenmaier, D. P.: Implications of Global Climate Change for Snowmelt Hydrology in the Twenty-First Century, Hydrological Processes, 23, 962–972, https://doi.org/10.1002/hyp.7201, 2009.

Barnett, T. P., Adam, J. C., and Lettenmaier, D. P.: Potential Impacts of a Warming Climate on Water Availability in Snow-Dominated Regions, Nature, 438, 303–309, https://doi.org/10.1038/nature04141, 2005.

Bavay, M., Grünewald, T., and Lehning, M.: Response of Snow Cover and Runoff to Climate Change in High Alpine Catchments of Eastern Switzerland, Advances in Water Resources, 55, 4–16, https://doi.org/10.1016/j.advwatres.2012.12.009, 2013.

Beniston, M., Stephenson, D. B., Christensen, O. B., Ferro, C. A. T., Frei, C., Goyette, S., Halsnaes, K., Holt, T., Jylhä, K., Koffi, B., Palutikof, J., Schöll, R., Semmler, T., and Woth, K.: Future Extreme Events in European Climate: An Exploration of Regional Climate Model Projections, Climatic Change, 81, 71–95, https://doi.org/10.1007/s10584-006-9226-z, 2007.

Beven, K., Cloke, H., Pappenberger, F., Lamb, R., and Hunter, N.: Hyperresolution Information and Hyperresolution Ignorance in Modelling the Hydrology of the Land Surface, Science China. Earth Sciences; Dordrecht, 58, 25–35, https://doi.org/http://dx.doi.org/10.1007/s11430-014-5003-4, 2015.

Beven, K. J. and Cloke, H. L.: Comment on "Hyperresolution Global Land Surface Modeling: Meeting a Grand Challenge for Monitoring Earth's Terrestrial Water" by Eric F. Wood et Al., Water Resources Research, 48, W01 801, https://doi.org/10.1029/2011WR010982, 2012.

Bierkens, M. F. P.: Global Hydrology 2015: State, Trends, and Directions, Water Resources Research, 51, 4923–4947, https://doi.org/10.1002/2015WR017173, 2015.

Bierkens, M. F. P., Bell, V. A., Burek, P., Chaney, N., Condon, L. E., David, C. H., De Roo, A., Döll, P., Drost, N., Famiglietti, J. S., Flörke, M., Gochis, D. J., Houser, P., Hut, R., Keune, J., Kollet, S., Maxwell, R. M., Reager, J. T., Samaniego, L., Sudicky, E., Sutanudjaja, E. H., Van De Giesen, N., Winsemius, H., and Wood, E. F.: Hyper-Resolution Global Hydrological Modelling: What Is Next?, Hydrological Processes, 29, 310–320, https://doi.org/10.1002/hyp.10391, 2015.

5 Blöschl, G., Nester, T., Komma, J., Parajka, J., and Perdigão, R. A. P.: The June 2013 Flood in the Upper Danube Basin, and Comparisons with the 2002, 1954 and 1899 Floods, Hydrology and Earth System Sciences, 17, 5197–5212, https://doi.org/10.5194/hess-17-5197-2013, 2013.

Brönnimann, S., Luterbacher, J., Ewen, T., Diaz, H. F., Stolarski, R. S., and Neu, U.: Climate Variability and Extremes during the Past 100 Years, Springer Science & Business Media, 2007.

10 Carpenter, T. M. and Georgakakos, K. P.: Intercomparison of Lumped versus Distributed Hydrologic Model Ensemble Simulations on Operational Forecast Scales, Journal of Hydrology, 329, 174–185, https://doi.org/10.1016/j.jhydrol.2006.02.013, 2006.

Clark, M. P., Bierkens, M. F. P., Samaniego, L., Woods, R. A., Uijlenhoet, R., Bennett, K. E., Pauwels, V. R. N., Cai, X., Wood, A. W., and Peters-Lidard, C. D.: The Evolution of Process-Based Hydrologic Models: Historical Challenges and the Collective Quest for Physical Realism, Hydrol. Earth Syst. Sci., 21, 3427–3440, https://doi.org/10.5194/hess-21-3427-2017, 2017.

15 Driessen, T. L. A., Hurkmans, R. T. W. L., Terink, W., Hazenberg, P., Torfs, P. J. J. F., and Uijlenhoet, R.: The Hydrological Response of the Ourthe Catchment to Climate Change as Modelled by the HBV Model, Hydrol. Earth Syst. Sci., 14, 651–665, https://doi.org/10.5194/hess-14-651-2010, 2010.

FOEN: Hydrological Data and Forecasts, http://www.hydrodaten.admin.ch/en/, federal Office for the Environment (FOEN), 2016.

Gao, X., Xu, Y., Zhao, Z., Pal, J. S., and Giorgi, F.: On the Role of Resolution and Topography in the Simulation of East Asia Precipitation, 20 Theoretical and Applied Climatology, 86, 173–185, https://doi.org/10.1007/s00704-005-0214-4, 2006.

Gupta, H. V., Kling, H., Yilmaz, K. K., and Martinez, G. F.: Decomposition of the Mean Squared Error and NSE Performance Criteria: Implications for Improving Hydrological Modelling, Journal of Hydrology, 377, 80–91, https://doi.org/10.1016/j.jhydrol.2009.08.003, 2009.

Gurtz, J., Zappa, M., Jasper, K., Lang, H., Verbunt, M., Badoux, A., and Vitvar, T.: A Comparative Study in Modelling Runoff and Its 25 Components in Two Mountainous Catchments, Hydrological Processes, 17, 297–311, https://doi.org/10.1002/hyp.1125, 2003.

Haddeland, I., Matheussen, B. V., and Lettenmaier, D. P.: Influence of Spatial Resolution on Simulated Streamflow in a Macroscale Hydrologic Model, Water Resources Research, 38, 29–1, https://doi.org/10.1029/2001WR000854, 2002.

Hunink, J. E., Eekhout, J. P. C., de Vente, J., Contreras, S., Droogers, P., and Baille, A.: Hydrological Modelling Using Satellite-Based Crop Coefficients: A Comparison of Methods at the Basin Scale, Remote Sensing, 9, 174, https://doi.org/10.3390/rs9020174, 2017.

30 Hurkmans, R. T. W. L., Terink, W., Uijlenhoet, R., Moors, E. J., Troch, P. A., and Verburg, P. H.: Effects of Land Use Changes on Streamflow Generation in the Rhine Basin, Water Resources Research, 45, https://doi.org/10.1029/2008WR007574, 2009.

Hurkmans, R. T. W. L., Terink, W., Uijlenhoet, R., Torfs, P., Jacob, D., and Troch, P. A.: Changes in Streamflow Dynamics in the Rhine Basin under Three High-Resolution Regional Climate Scenarios, Journal of Climate, 23, 679–699, https://doi.org/10.1175/2009JCLI3066.1, 2010.

35 Immerzeel, W. W., Van Beek, L. P. H., Konz, M., Shrestha, A. B., and Bierkens, M. F. P.: Hydrological Response to Climate Change in a Glacierized Catchment in the Himalayas, Climatic Change, 110, 721–736, https://doi.org/10.1007/s10584-011-0143-4, 2012.

Jacob, D., Petersen, J., Eggert, B., Alias, A., Christensen, O. B., Bouwer, L. M., Braun, A., Colette, A., Déqué, M., Georgievski, G., Georgopoulou, E., Gobiet, A., Menut, L., Nikulin, G., Haensler, A., Hempelmann, N., Jones, C., Keuler, K., Kovats, S., Kröner, N., Kotlarski,

S., Kriegsmann, A., Martin, E., Van Meijgaard, E., Moseley, C., Pfeifer, S., Preuschmann, S., Radermacher, C., Radtke, K., Rechid, D., Rounsevell, M., Samuelsson, P., Somot, S., Soussana, J.-F., Teichmann, C., Valentini, R., Vautard, R., Weber, B., and Yiou, P.: EURO-CORDEX: New High-Resolution Climate Change Projections for European Impact Research, Regional Environmental Change, 14, 563–578, https://doi.org/10.1007/s10113-013-0499-2, 2014.

Jarvis, A., Reuter, H., Nelson, A., and Guevara, E.: Hole-Filled SRTM for the Globe Version 4, Available from the CGIAR-CSI SRTM 90m Database, http://srtm.csi.cgiar.org, 2008.

Jolly, W. M., Dobbertin, M., Zimmermann, N. E., and Reichstein, M.: Divergent Vegetation Growth Responses to the 2003 Heat Wave in the Swiss Alps, Geophysical Research Letters, 32, L18 409, https://doi.org/10.1029/2005GL023252, 2005.

Kumar, R., Musuuza, J. L., Van Loon, A. F., Teuling, A. J., Barthel, R., Ten Broek, J., Mai, J., Samaniego, L., and Attinger, S.: Multiscale Evaluation of the Standardized Precipitation Index as a Groundwater Drought Indicator, Hydrol. Earth Syst. Sci., 20, 1117–1131, https://doi.org/10.5194/hess-20-1117-2016, 2016.

Leung, L. R. and Qian, Y.: The Sensitivity of Precipitation and Snowpack Simulations to Model Resolution via Nesting in Regions of Complex Terrain, Journal of Hydrometeorology, 4, 1025–1043, 2003.

Lobligeois, F., Andréassian, V., Perrin, C., Tabary, P., and Loumagne, C.: When Does Higher Spatial Resolution Rainfall Information Improve Streamflow Simulation? An Evaluation Using 3620 Flood Events, Hydrology and Earth System Sciences, 18, 575–594, https://doi.org/10.5194/hess-18-575-2014, 2014.

Lucas-Picher, P., Wulff-Nielsen, M., Christensen, J. H., Adalgeirsdóttir, G., Mottram, R., and Simonsen, S. B.: Very High Resolution Regional Climate Model Simulations over Greenland: Identifying Added Value, Journal of Geophysical Research: Atmospheres, 117, D02 108, https://doi.org/10.1029/2011JD016267, 2012.

Luterbacher, J., Dietrich, D., Xoplaki, E., Grosjean, M., and Wanner, H.: European Seasonal and Annual Temperature Variability, Trends, and Extremes Since 1500, Science, 303, 1499–1503, https://doi.org/10.1126/science.1093877, 2004.

Lutz, A. F., Immerzeel, W. W., Gobiet, A., Pellicciotti, F., and Bierkens, M. F. P.: Comparison of Climate Change Signals in CMIP3 and CMIP5 Multi-Model Ensembles and Implications for Central Asian Glaciers, Hydrol. Earth Syst. Sci., 17, 3661–3677, https://doi.org/10.5194/hess-17-3661-2013, 2013.

Lutz, A. F., Immerzeel, W. W., Shrestha, A. B., and Bierkens, M. F. P.: Consistent Increase in High Asia's Runoff Due to Increasing Glacier Melt and Precipitation, Nature Climate Change, 4, 587–592, https://doi.org/10.1038/nclimate2237, 2014.

Lutz, A. F., Immerzeel, W. W., Kraaijenbrink, P. D. A., Shrestha, A. B., and Bierkens, M. F. P.: Climate Change Impacts on the Upper Indus Hydrology: Sources, Shifts and Extremes, PLOS ONE, 11, e0165 630, https://doi.org/10.1371/journal.pone.0165630, 2016.

McKay, M. D., Beckman, R. J., and Conover, W. J.: A Comparison of Three Methods for Selecting Values of Input Variables in the Analysis of Output from a Computer Code, Technometrics, 21, 239–245, https://doi.org/10.2307/1268522, 1979.

Melsen, L., Teuling, A., Torfs, P., Zappa, M., Mizukami, N., Clark, M., and Uijlenhoet, R.: Representation of Spatial and Temporal Variability in Large-Domain Hydrological Models: Case Study for a Mesoscale Pre-Alpine Basin, Hydrology and Earth System Sciences, 20, 2207–2226, https://doi.org/10.5194/hess-20-2207-2016, 2016a.

Melsen, L. A., Teuling, A. J., Torfs, P. J. J. F., Uijlenhoet, R., Mizukami, N., and Clark, M. P.: HESS Opinions: The Need for Process-Based Evaluation of Large-Domain Hyper-Resolution Models, Hydrology and Earth System Sciences, 20, 1069–1079, https://doi.org/10.5194/hess-20-1069-2016, 2016b.

MeteoSwiss: Daily Mean, Minimum and Maximum Temperature: TabsD, TminD, TmaxD, Tech. rep., Federal Office of Meteorology and Climatology (MeteoSwiss), 2013.

MeteoSwiss: Daily Precipitation: RhiresD, Tech. rep., Federal Office of Meteorology and Climatology (MeteoSwiss), 2016.

MeteoSwiss: Très Chaud à La Fin Du Mois de Mai, http://www.meteosuisse.admin.ch/home/actualite/meteosuisse-blog.subpage.html/fr/data/blogs/2017/5/mai-mit-heissem-ende.html, 2017.

Middelkoop, H., Daamen, K., Gellens, D., Grabs, W., Kwadijk, J. C., Lang, H., Parmet, B. W., Schädler, B., Schulla, J., and Wilke, K.: Impact of Climate Change on Hydrological Regimes and Water Resources Management in the Rhine Basin, Climatic Change, 49, 105–128, 2001.

Peters-Lidard, C. D., Clark, M., Samaniego, L., Verhoest, N. E. C., van Emmerik, T., Uijlenhoet, R., Achieng, K., Franz, T. E., and Woods, R.: Scaling, Similarity, and the Fourth Paradigm for Hydrology, Hydrol. Earth Syst. Sci., 21, 3701–3713, https://doi.org/10.5194/hess-21-3701-2017, 2017.

Pryor, S. C., Nikulin, G., and Jones, C.: Influence of Spatial Resolution on Regional Climate Model Derived Wind Climates, Journal of Geophysical Research: Atmospheres, 117, D03 117, https://doi.org/10.1029/2011JD016822, 2012.

Sánchez, E., Gallardo, C., Gaertner, M., Arribas, A., and Castro, M.: Future Climate Extreme Events in the Mediterranean Simulated by a Regional Climate Model: A First Approach, Global and Planetary Change, 44, 163–180, https://doi.org/10.1016/j.gloplacha.2004.06.010, 2004.

Schaefli, B., Hingray, B., and Musy, A.: Climate Change and Hydropower Production in the Swiss Alps: Quantification of Potential Impacts and Related Modelling Uncertainties, Hydrol. Earth Syst. Sci., 11, 1191–1205, https://doi.org/10.5194/hess-11-1191-2007, 2007.

Schmidli, J. and Frei, C.: Trends of Heavy Precipitation and Wet and Dry Spells in Switzerland during the 20th Century, International Journal of Climatology, 25, 753–771, https://doi.org/10.1002/joc.1179, 2005.

Seneviratne, S. I., Lehner, I., Gurtz, J., Teuling, A. J., Lang, H., Moser, U., Grebner, D., Menzel, L., Schroff, K., Vitvar, T., and Zappa, M.: Swiss Prealpine Rietholzbach Research Catchment and Lysimeter: 32 Year Time Series and 2003 Drought Event, Water Resources Research, 48, W06 526, https://doi.org/10.1029/2011WR011749, 2012.

Sheffield, J. and Wood, E. F.: Global Trends and Variability in Soil Moisture and Drought Characteristics, 1950–2000, from Observation-Driven Simulations of the Terrestrial Hydrologic Cycle, Journal of Climate, 21, 432–458, https://doi.org/10.1175/2007JCLI1822.1, 2008.

Sheffield, J., Wood, E. F., and Roderick, M. L.: Little Change in Global Drought over the Past 60 Years, Nature, 491, 435–438, https://doi.org/10.1038/nature11575, 2012.

Speich, M. J. R., Bernhard, L., Teuling, A. J., and Zappa, M.: Application of Bivariate Mapping for Hydrological Classification and Analysis of Temporal Change and Scale Effects in Switzerland, Journal of Hydrology, 523, 804–821, https://doi.org/10.1016/j.jhydrol.2015.01.086, 2015.

Stahl, K., Weiler, M., Kohn, I., Freudiger, D., Seibert, J., Vis, M., Gerlinger, K., and Bohm, M.: The Snow and Glacier Melt Components of Streamflow of the River Rhine and Its Tributaries Considering the Influence Climate Change, Tech. Rep. I-25, CHR, 2016.

Terink, W., Lutz, A. F., Simons, G. W. H., Immerzeel, W. W., and Droogers, P.: SPHY v2.0: Spatial Processes in HYdrology, Geosci. Model Dev., 8, 2009–2034, https://doi.org/10.5194/gmd-8-2009-2015, 2015.

Teuling, A. J., Van Loon, A. F., Seneviratne, S. I., Lehner, I., Aubinet, M., Heinesch, B., Bernhofer, C., Grünwald, T., Prasse, H., and Spank, U.: Evapotranspiration Amplifies European Summer Drought, Geophysical Research Letters, 40, 2071–2075, https://doi.org/10.1002/grl.50495, 2013.

Theurillat, J.-P. and Guisan, A.: Potential Impact of Climate Change on Vegetation in the European Alps: A Review, Climatic Change, 50, 77–109, https://doi.org/10.1023/A:1010632015572, 2001.

Van Huijgevoort, M. H. J., Van Lanen, H. A. J., Teuling, A. J., and Uijlenhoet, R.: Identification of Changes in Hydrological Drought Characteristics from a Multi-GCM Driven Ensemble Constrained by Observed Discharge, Journal of Hydrology, 512, 421–434, https://doi.org/10.1016/j.jhydrol.2014.02.060, 2014.

Van Tiel, M., Teuling, A. J., Wanders, N., Vis, M. J. P., Stahl, K., and Van Loon, A. F.: The Role of Glacier Changes and Threshold

5   Definition in the Characterisation of Future Streamflow Droughts in Glacierised Catchments, Hydrol. Earth Syst. Sci., 22, 463–485, https://doi.org/10.5194/hess-22-463-2018, 2018.

Verbunt, M., Gurtz, J., Jasper, K., Lang, H., Warmerdam, P., and Zappa, M.: The Hydrological Role of Snow and Glaciers in Alpine River Basins and Their Distributed Modeling, Journal of Hydrology, 282, 36–55, https://doi.org/10.1016/S0022-1694(03)00251-8, 2003.

Wolf, A. T., Natharius, J. A., Danielson, J. J., Ward, B. S., and Pender, J. K.: International River Basins of the World, International Journal

10   of Water Resources Development, 15, 387–427, https://doi.org/10.1080/07900629948682, 1999.

Wong, W. K., Beldring, S., Engen-Skaugen, T., Haddeland, I., and Hisdal, H.: Climate Change Effects on Spatiotemporal Patterns of Hydroclimatological Summer Droughts in Norway, Journal of Hydrometeorology, 12, 1205–1220, https://doi.org/10.1175/2011JHM1357.1, 2011.

Wood, E. F., Roundy, J. K., Troy, T. J., Van Beek, L. P. H., Bierkens, M. F. P., Blyth, E., De Roo, A., Döll, P., Ek, M., Famiglietti, J., Gochis,

15   D., Van De Giesen, N., Houser, P., Jaffé, P. R., Kollet, S., Lehner, B., Lettenmaier, D. P., Peters-Lidard, C., Sivapalan, M., Sheffield, J., Wade, A., and Whitehead, P.: Hyperresolution Global Land Surface Modeling: Meeting a Grand Challenge for Monitoring Earth's Terrestrial Water, Water Resources Research, 47, W05 301, https://doi.org/10.1029/2010WR010090, 2011.

WSL: CORINE Land Cover Switzerland, http://www.wsl.ch/fe/landschaftsdynamik/projekte/corine_landcover_update/index_EN, swiss Federal Institute for Forest, Snow and Landscape Research (WSL), 2016.

20   Zappa, M. and Kan, C.: Extreme Heat and Runoff Extremes in the Swiss Alps, Natural Hazards and Earth System Science, 7, 375–389, 2007.

Zhu, C., Byrd, R. H., Lu, P., and Nocedal, J.: Algorithm 778: L-BFGS-B: Fortran Subroutines for Large-Scale Bound-Constrained Optimization, ACM Trans. Math. Softw., 23, 550–560, https://doi.org/10.1145/279232.279236, 1997.